Baryshnikova, Kseniia; Filonov, Dmitriy; Simovski, Constantin; Evlyukhin, Andrey; Kadochkin, Alexey; Nenasheva, Elizaveta; Ginzburg, Pavel; Shalin, Alexander S.

Giant magnetoelectric field separation via anapole-type states in high-index dielectric structures

Published in:
Physical Review B

DOI:
10.1103/PhysRevB.98.165419

Published: 15/10/2018

Document Version
Publisher's PDF, also known as Version of record

Please cite the original version:
Baryshnikova, K., Filonov, D., Simovski, C., Evlyukhin, A., Kadochkin, A., Nenasheva, E., Ginzburg, P., & Shalin, A. S. (2018). Giant magnetoelectric field separation via anapole-type states in high-index dielectric structures. *Physical Review B*, *98*(16), Article 165419. https://doi.org/10.1103/PhysRevB.98.165419

Giant magnetoelectric field separation via anapole-type states in high-index dielectric structures

Kseniia Baryshnikova,[1,*] Dmitriy Filonov,[1,2] Constantin Simovski,[1,3] Andrey Evlyukhin,[1,4,5] Alexey Kadochkin,[1,6] Elizaveta Nenasheva,[7] Pavel Ginzburg,[1,2] and Alexander S. Shalin[1]

[1]*ITMO University, Saint Petersburg 197101, Russia*

[2]*School of Electrical Engineering, Tel Aviv University, Tel Aviv 69978, Israel*

[3]*Department of Radio Science and Engineering, Aalto University, P.O. Box 13000, FI-00076 Aalto, Finland*

[4]*Laser Zentrum Hannover e.V., Hollerithallee 8, D-30419 Hannover, Germany*

[5]*Moscow Institute of Physics and Technology, 9 Institutsky Lane, Dolgoprudny 141700, Russia*

[6]*Ulyanovsk State University, Ulyanovsk 432017, Russia*

[7]*Giricond Research Institute, Ceramics Co., Ltd., Saint Petersburg 194223, Russia*

(Received 1 June 2018; revised manuscript received 14 September 2018; published 15 October 2018)

The value of the spatial separation between electric and magnetic fields in an electromagnetic wave is fundamentally constrained by the nonlocal nature of Maxwell's equations. While electric and magnetic energy densities in a plane wave propagating in vacuum are equal at each point of space, carefully designed photonic structures can lead to a spatial separation of the electric and magnetic fields. Here, a set of high-index dielectric tubes was proposed and demonstrated to deliver a record high spatial separation overcoming the free space scenario by more than three orders of magnitude. The separation effect in the structure is enabled by the near-field interference between an incident radiation and anapole-type states designed by tuning geometrical parameters of coupled dielectric tubes. Near-field scanning of field components within the void structure confirmed the predicted values of magnetoelectric separation. Furthermore, the near-field interference concept in application to magnetoelectric separation can be employed in a range of spectroscopic tests, where objects (e.g., atoms with magnetic optical transitions) can be placed in voids. Devices providing tunable separation between the fields are important in nano-optics for magnetic particle or atom detection and trapping, in medicine for magnetic resonance imaging, etc.

DOI: 10.1103/PhysRevB.98.165419

I. INTRODUCTION

A wide range of magnetic phenomena can be treated as relativistic corrections to electrostatic effects [1]. As a result, magnetic contributions are usually orders of magnitude weaker than their electrical counterparts. For example, many fundamental light-matter interaction phenomena are driven by electrical dipole transitions, while other multipoles play only a minor role [2]. Qualitative analysis shows that the ratio between magnetic and electric dipole transitions in atoms scales with fine-structure constant α (see, e.g., Ref. [3]). Nevertheless, the ability to efficiently probe magnetic lines in luminescent transitions plays a key role in spectroscopic and metrological applications. Quite a substantial effort was devoted to the investigations of magnetic transitions in atoms and molecules (see, e.g., Refs. [4–6]), shining light on their internal structure. One of the major challenges in the optical spectroscopic analysis of magnetic contributions is to separate them from other processes that may be orders of magnitude stronger. A reliable detection of magnetic optical transitions requires the ratio of the electric and magnetic local fields in order to obtain values of inverse fine-structure constant α [5,7], in fluorescent imaging [8] including magnetic fluorescence enhancement [9,10], and allows for tailoring the magnetic transition rates [11]. Suppression of the electric field makes optically small objects without magnetic response invisible [12–14].

Novel devices providing tunable high-quality separation between fields are in high demand for a variety of applications, e.g., sensing and trapping of magnetic particles and atoms, magnetic transition spectroscopy, etc. [5,15–17]. Moreover, the proposed design seems to be very promising for magnetic resonance imaging applications, where a parasitic electric field leads to the distortion and low contrast of pictures. In contrast, an amplified magnetic field can increase the quality [18,19].

So, the enhancement of a magnetic local field and suppression of an electric one in a predefined spatial region in a certain frequency range is a practically important task. In order to achieve this local effect without absorption one needs to separate the local maxima of the electric and magnetic fields in space. The issue to be resolved in order to perform this separation is inherent coupling between the electric and magnetic components of light governed by Maxwell's equations.

Experimental attempts on magnetoelectrical separation have roots back to 1930, where nullifying the electrical field was achieved at radio frequencies in a node of a standing wave created by a reflection from a mirror [20]. In this frequency range, the standing-wave technique for separating electric and magnetic fields is nowadays a commonplace. As to optical range, the standing-wave interferometric effects were also utilized in several applications, such as chirality enhancement [21], Fourier spectrometry [22], and a few others. However,

*k.baryshnikova@optomech.ifmo.ru

practical constraints, such as high precision in mirror positioning, optical alignment, and low tolerance to fabrication inaccuracies, together with fundamentally very steep gradients of the electrical fields at a node, set limitations on applicability of this approach for the aforementioned purposes [23].

Another technique for obtaining the spatial separation is the formation of a wave beam with azimuthal polarization. On the axis of this wave beam, the electric field vanishes and the magnetic field is longitudinally directed and maximal. Such beams can propagate in an optical fiber and keep in free space behind an axicon lens, since their diffraction in free space is suppressed [24]. This technique was used in order to observe magnetic optical transitions in Ref. [5]. However, obtaining such wave beams in an optical fiber is demanding—it requires special, and very expensive, equipment [23]. Therefore, an alternative technique of electric and magnetic field separation is required. Specifically, it is desirable to have a simple passive structure that enhances the local magnetic field and suppresses the electric one over a sufficiently substantial area under plane-wave illumination.

At radio frequencies, the enhancement of the local magnetic field is achievable in magnetic materials. In the optical range, where the natural magnetism vanishes, a strong magnetic response can be achieved in some metamaterials [25,26]. One promising approach relies on the employment of higher-order Mie resonances in high-index dielectric nanoparticles (see, e.g., Refs. [27–31]). Tuning geometrical parameters of those particles enables achieving many remarkable properties, such as spectral overlapping of multipole resonances [32,33], ultrahigh-quality Fano resonances [34,35], directive scattering [36–39], invisibility, and cloaking [40,41]. Multiparticle high-index structures open a venue for flexible control over the electric and magnetic near-fields and their gradients. For example, the dimers formed by high-index cubes were shown to enhance the magnetic field intensity by more than two orders of magnitude [42]. Dielectric tubes were also investigated in the context of the local magnetic field concentration [38]. However, no significant weakening of the electric field was provided. Therefore, we aim to enhance the magnetic field and to cancel the electric one, which requires a different approach. In particular, magnetic Mie resonances in high-index dielectric particles rely on retardation effects, and, as a result, the phase shift of an incident wave over the particle results in the unavoidable excitation of other multipoles even though they are not under resonant conditions. Nullifying the electrical field even at the particle center is possible only if the electric field of induced multipoles compensates the incident electric field. Moreover, to achieve the enhancement of the magnetic field at the same area it is necessary to engineer magnetic multipoles and their resonances. Consequently, careful analysis of the multipole contributions is of crucial importance to achieve the desired goal.

This analysis will be done below and the auxiliary dielectric tubular structure will be designed to realize giant magnetoelectric field separation. Due to the coaxial shape of the particles in the structure, the area with the efficient magnetoelectric separation will be externally accessible.

The paper is organized as follows: a multipole decomposition of the polarization currents in a high-index dielectric tube is studied and utilized for achieving high magnetoelectric field separation. The multipole moments are optimized to obtain near-zero electric field and sufficient magnetic field inside the tube. The next stage involves the multipole design in arrays of such dielectric tubes. Since the multipole modes have significant spectral overlap with each other, a minimized, yet sufficient, number of geometrical degrees of freedom is required. Finally, proof of the concept experiment at gigahertz spectral range will be demonstrated to support the theoretic predictions.

II. NEAR-FIELD INTERFERENCE BETWEEN MULTIPOLES

The dimensionless magnetoelectric separation factor K we aim to maximize at a certain frequency is defined as

$$K(\vec{r}) = \eta_0 \left| \frac{\vec{H}(\vec{r})}{\vec{E}(\vec{r})} \right|, \tag{1}$$

where η_0 is the free space wave impedance, while $\vec{H}(\vec{r})$ and $\vec{E}(\vec{r})$ are local magnetic and electric fields correspondingly. To achieve the separation effect we, in the first stage, suggest using a dielectric nanotube. Coaxial tubes are promising candidates, since the number of geometrical parameters required for their parametrization is sufficient for the efficient resonant tuning on the one hand, and the void geometry provides the direct access to the local field, where high K is tailored, on the other hand [Fig. 1(a)]. The sketch shows the schematic for making the electrical field close to zero at the center of the structure, while the magnetic field is locally maximal, leading to high values of the target coefficient $K(r = 0)$ (or just K hereafter).

The key effect, responsible for the magnetoelectric separation, is the emergence of the anapole state, as will be shown hereafter. Since the anapole is not a true eigenmode within the multipole decomposition, but rather the combination of dipolar and toroidal moments given by Eqs. (A2), (A7), and (A8) in the Appendix (see also Ref. [40]), it is referred to as a "state" and not as a "mode." Figure 1(b) illustrates how this state rises from nonresonant modes. The concept of the anapole state further extends: anapole-type states are defined as states with arbitrary excited multipoles and vanishing total dipole polarization $\mathbf{D} \approx 0$ (see the Appendix). This family of states demonstrates a suppression of the combination of electric and toroidal dipoles down to several orders of magnitude in comparison to the electric dipolar moment $\mathbf{p}$. The proposed effect is obtained owing to additional higher multipoles interference and, as a result, a pronounced resonant minimum in the scattering properties can be achieved. Furthermore, those anapole-type states can be designed to have close to zero total electrical field at the central region. There the scattered electric field almost compensates the incident one, while the local magnetic field is maximized [Fig. 1(b)]. If those states are designed to have proper amplitudes and phases, the electric field at the center of the system will vanish. At the same time, the existence of the magnetic dipole mode can be constrained by this method and it will provide the enhancement of the magnetic field compared to that of the incident wave. This enhancement occurs in the void, and K achieves its absolute maximum.

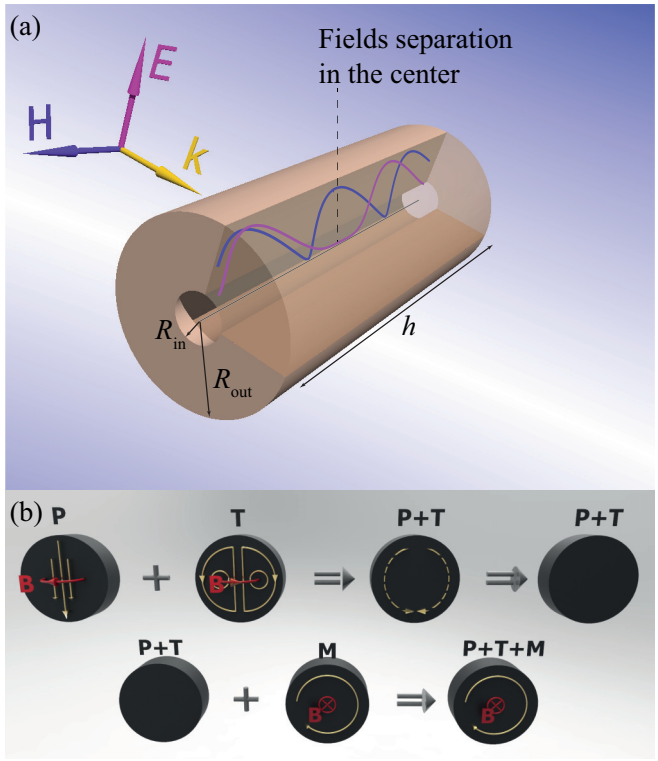

FIG. 1. Magnetoelectric separation concept in all-dielectric structures. (a) Schematics of a dielectric tube illuminated with a plane wave from the side. Purple and magenta lines represent distributions of magnetic and electric fields along the symmetry axis, respectively. (b) Schematics of multipolar decomposition in a particle; **P**, **T,** and **M** stand for electric dipole, electric toroidal dipole, and magnetic dipole moments; red lines represent magnetic field **B**; golden lines represent polarization currents.

It is necessary to provide here some explanations on the nullifying of the electric field in the center of the structure due to the interaction of the displacement currents corresponding to the electric dipole and toroidal dipole moments. Multipole moments, which define the structure's optical response, are integrals of some functions of electric field vector and coordinates inside the structure's volume. Electric dipole **P** and toroidal dipole **T** moments can be expressed as integrals over the fields inside the nanoparticles [see Eqs. (A2) and (A7)]. It is obvious that **P** and **T** can have equal values for different integrands and, therefore, for different distributions of the electric field **E** inside objects. For the particles with low aspect ratio (disks) the anapole state can correlate to the case in which the electric field is enhanced in the particle center, as it is shown in Ref. [40]; for other particles the field could have another map [43]. In our case of the high aspect ratio cylinders with coaxial voids the distribution of the electric field has the particular form with the vanishing values in the particle's center [Fig. 1(b)].

III. PROPOSED ALL-DIELECTRIC STRUCTURES AND NUMERICAL RESULTS

Hereafter, the anapole-type states in dielectric tubes are revealed and analyzed numerically. Simultaneously, the separation coefficient K at the center of the structure will be maximized. It is worth noting, however, that for the side illumination of the structure [Fig. 1(a)] the maximal value of $K(\vec{r})$ could be obtained at the slightly offset point owing to retardation effects. Nevertheless, for convenience, the geometrical center of the particle will be taken as a reference point. The parameters of the basic building block are R_{out} and R_{in}—the outer and inner radii, correspondingly—while h is the height [Fig. 1(a)]. This type of the incident wave polarization was chosen due to the effective excitation of a magnetic hot spot as is shown here [7]. Let us first numerically optimize the separation coefficient in the system and than the multipole-based explanations will be given.

An isolated silicon nanotube was considered first and the magnetoelectric separation was maximized by running numerical optimization over all the three geometrical parameters. Relatively high separation values of K (as high as 4000) were observed at several geometries for silicon tubes, which, however, demand significant aspect ratios $h/2R_{out}$ and $h/2R_{in}$ to exceed values of 10. Being valuable from the theoretical standpoint, those parameters are challenging to achieve with the existing fabrication technologies. High aspect ratios could be obtained by cascading several identical particles on top of each other. In this case, the separation distance between tubes serves as an additional valuable tuning parameter, capable of maximizing the magnetoelectric separation coefficient and the magnetic field inside the void.

Next, the structure composed of three aligned silicon nanotubes [Fig. 2(a)] is considered. It is worth noting that a pair of tubes was tested, but did not show significant improvement of K with respect to a single tube. A structure of three tubes was optimized over all the geometrical parameters including the separation distance between the tube edges d. The results for the optimized structure with the parameters $R_{out} = 198\,\text{nm}$, $h = 181\,\text{nm}$, $R_{in} = 30\,\text{nm}$, and $d = 26\,\text{nm}$ appear in Fig. 2. The separation coefficient as high as $K = 5730$, with the local magnetic field enhancement higher than 10, is obtained for the illumination wavelength of 808 nm. This value is one order of magnitude higher than the one reported in Ref. [5], where the structure was illuminated by an azimuthally polarized light beam. Also we want to stress that the volume at which a sufficient spatial separation takes place is comparable with the nanoparticle size: it is almost all the volume inside the central void. Amplitudes of magnetic and electric fields within the three tubes' structure appear in Figs. 2(b) and 2(c). It can be seen that the region of the maximal magnetic field is located at the center of the structure, where the electric field is minimized. The field maps have slight asymmetry with respect to the axis of the tubes owing to the phase accumulation effect mentioned before.

In order to verify the anapole-type state's contribution to the predicted magnetoelectric separation effect, multipolar decomposition of the fields is performed.

IV. MULTIPOLE DECOMPOSITION

Cartesian multipoles and their contributions to the total scattering cross section can be obtained in the irreducible representations [44,46]. Relevant expressions for the calculations of the multipoles and their contributions to the scattering cross-section appear in the Appendix. Figure 3(a) summarizes

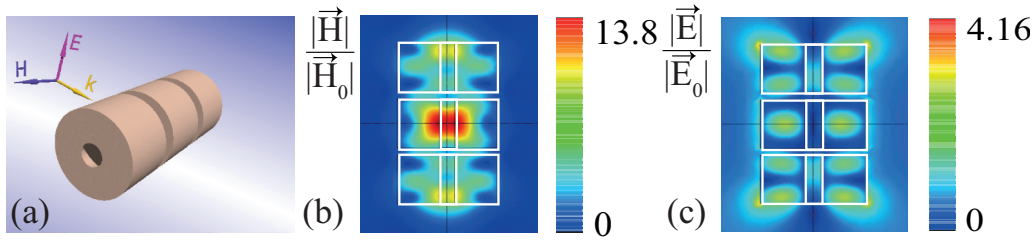

FIG. 2. Magnetoelectric separation in the three silicon tubes system. (a) Schematics of the structure. (b) Magnetic field amplitude enhancement with respect to the free space component of a plane wave. (c) Electric field amplitude enhancement with respect to the free space component of a plane wave. Parameters of the system: $R_{out} = 198$ nm, $h = 181$ nm, $R_{in} = 30$ nm, $d = 26$ nm, illumination wavelength 808 nm, magnetoelectric separation coefficient $K = 5730$.

the results for the multipole decomposition spectra, obtained for the investigated structure. The total electric dipole spectrum (being the sum of the electric dipole and electric toroidal dipole) shows a dip at the same wavelength (marked by the vertical dashed line), where the maximal magnetoelectric separation is observed. Thus, the maximal separation is achieved at the frequency of the anapole-type state (as it will be shown further, the maximal separation coefficient always takes place at the frequency of the anapole-type state). At the axis of the system the field of the electric dipole moment destructively interferes with that of the toroidal moment, and the difference of their amplitude is small enough to nearly compensate each other. In this case the electric field in the nanoparticle center is suppressed down to zero as it is shown in Fig. 1. In the inset of Fig. 3(b) we may see the phase shift between the moments at the wavelength of the anapole-type state (808 nm). Note that this state turns out to be within the band of the magnetodipole resonance (but *does not* coincide with the maximum), which, as was already mentioned, helps to increase K. For other design parameters, as it will be shown further, the anapole-type state may be far from the magnetic dipole resonance on the frequency axis; however, maximal K corresponds, namely, to the anapole-type state, where the total electric field is suppressed in the axial region (which proves that separation is not provided by magnetic dipole resonance only). Meanwhile, without the enhancement of the local magnetic field granted by the magnetic resonance this value is much lower than in the present case. In our experiment we demonstrate specifically the structure the magnetic dipole resonance of which is shifted from that anapole-type state.

V. EXPERIMENT

Fabrication of nanoscale silicon particles of coaxial shapes could be done with advanced nanolithography techniques. However, in this paper we provide a proof-of-concept experiment in the microwave spectral range, which is possible due to the scalability of Maxwell's equations and is common practice for emulating optical experiments of a different complexity [45]. Mature microwave technology offers numerous tools for advanced analysis of electromagnetic fields.

Dielectric tubes are fabricated from MgO-TiO_2 ceramics, which has dielectric permittivity = 16 roughly replicating properties of silicon in the visible range. Three identical tubes with $h = 43.4$ mm, inner radii $R_{in} = 8.1$ mm, and outer radii $R_{out} = 28.8$ mm are under consideration. The optimal distance between the tubes is found to be 8 mm. Inner and outer radii of the tubes are predefined by the fabrication

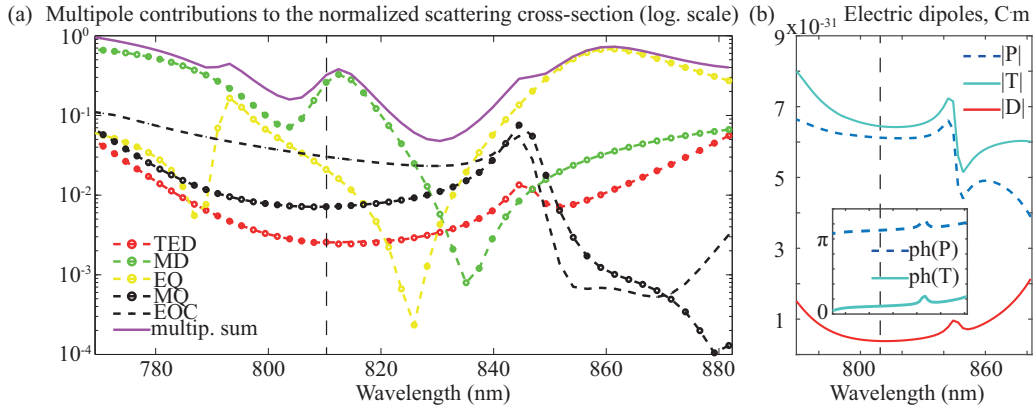

FIG. 3. (a) Multipole decomposition spectra (logarithmic scale). TED, total electric dipole; MD, magnetic dipole; EQ, electric quadrupole; MQ, magnetic quadrupole; EOC, electric octupole; the purple line stands for the sum of the mentioned multipoles. (b) Spectral dependencies of the electric dipole (dashed blue line), the toroidal dipole (aquamarine line), and the total electric dipole (red line) moments' absolute values. Inset: Phases of the electric dipole (dashed blue line) and the toroidal dipole (aquamarine line) moments. All graphs correspond to the case of the three silicon tubes structure with the parameters $R_{out} = 198$ nm, $h = 181$ nm, $R_{in} = 30$ nm, and $d = 26$ nm. The vertical dashed line corresponds to the wavelength of maximal magnetoelectric separation with $K = 5730$.

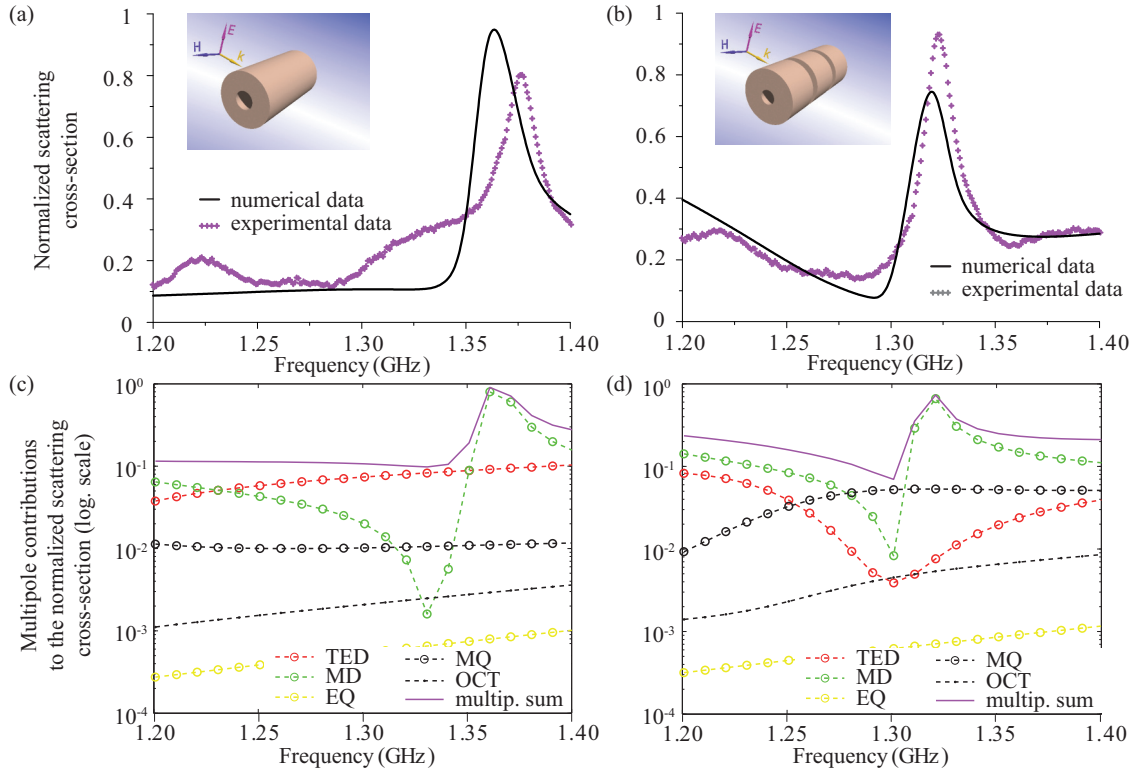

FIG. 4. Magnetoelectric separation in ceramic tubes at gigahertz frequency range. The left column shows the results for touching tubes (one solid structure, inset in panel a). The right column shows the results for 8-mm distance between the tubes (inset in panel b), for which the maximal magnetoelectric separation is achieved. (a, b) Normalized scattering cross-section spectra in arbitrary units: experimental (purple dotted line) and numerical (black solid line). (c, d) Multipole decomposition for obtaining the normalized scattering cross-section spectra. Data are presented in the logarithmic scale. Abbreviations are similar to Fig. 3.

aspects (sizes of the forms for compression and polishing) reducing the available optimization parameters. The plane-wave excitation is generated by radiating a wave from a rectangular horn antenna connected to the transmitting port of a Vector Network Analyzer (VNA E8362B). The tubes are located at the far-field of the antenna (the distance is 2.5 m), and a second (identical) horn is placed on the optical axis and serves as a receiver.

As a result, the maximal magnetoelectric separation under those fabrication constraints is found to be 600. Figure 4 summarizes the experimental results and numerical predictions. Full wave numerical simulations of the entire structure are obtained with CST Microwave Studio. In order to underline the importance of the separation distance, which controls the coupling between the tubes and multipole response of the system, two different geometries are compared. The first one (left column of Fig. 4) is the case of touching objects ($d = 0$ mm), while the second one is $d = 8$ mm (optimal design, right column of Fig. 4). It can be seen that the long tube without the gaps (first case) does not show any dip in the total dipole moment spectrum (electric dipole plus electric toroidal dipole), while in the optimized geometry the toroidal dipole cancels the dipole mode, giving rise to an anapole-type state at the special wavelength. The experimental scattering cross-section spectra are obtained with the employment of the optical theorem and extraction of the data from the measured values of the forward scattering [Figs. 4(a) and 4(b)]. The difference of the experimental and numerical scattering cross-sections is caused by small variations of the samples' geometrical parameters due to the fabrication imperfectness. A small nonzero gap between the touching tubes (theoretically $d = 0$ mm) causes additional deviations from the numerical prediction in Fig. 4(a), where the difference is sufficiently more significant. The multipole decomposition analysis clearly shows that the strong magnetic dipole resonance predominates the other multipoles and dictates the shape of the scattering cross-section in both the cases [green circles line in Figs. 4(c) and 4(d)]. Increasing the distance between the tubes shifts the scattering cross-section peak to lower frequencies. In the case of $d = 8$ mm one can see the strong dip before the resonant frequency. This dip corresponds not only to the minimum of the total electric dipole moment [see red circles line in Fig. 4(d)] but also to the minimum of the magnetic dipole moment. Numerical simulations also show that the maximal separation coefficient is observed at this frequency. This once again proves that the separation effect does not solely rely on the magnetic dipole resonance effect but corresponds to the anapole-type state (the minimum total electric dipole contribution in the scattering), in full correspondence with the previously discussed optical domain scenario.

In order to observe the magnetoelectric separation effect experimentally, the electric and the magnetic fields inside the structures are scanned with the near-field probes.

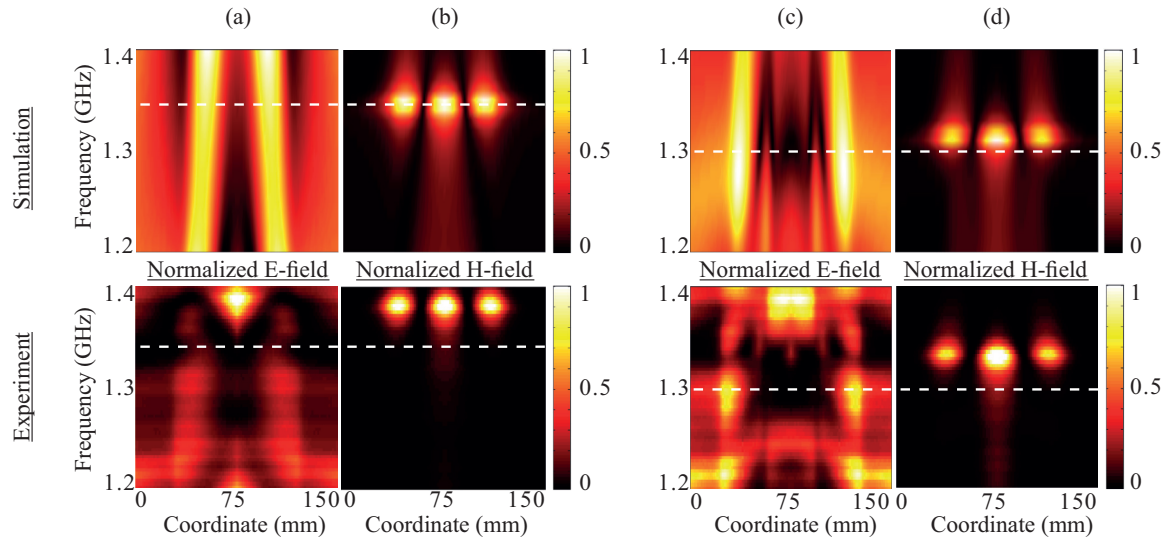

FIG. 5. Normalized electric (a, c) and magnetic (b, d) field amplitudes on the structure's symmetry axis, as a function of the coordinate and frequency. The left column (a, b) shows results for touching tubes. The right column (c, d) shows results for 8-mm distance between the tubes, with which the maximal magnetoelectric separation is achieved. The frequency corresponding to the best theoretical value of the separation is marked by a white dashed line.

Experimental data show qualitative agreement with the numerical modeling (see Fig. 5; fields in both cases were normalized to the maximum). The results for the cases of the touching tubes and the tubes with the optimal separation are different. In the first case the electric field at the center of the structure does not go down below 30% of its absolute maximum, while in the second case it drops by 95% of its initial value offering $K \approx 600$, which is nearly the same as numerical simulation predicts. Horizontal white lines in Fig. 5 highlight the frequency of the maximal separation effect.

In the case of $d = 0$ mm [Figs. 5(a) and 5(b)], the maximal separation corresponds to the magnetic dipole resonance frequency and the separation coefficient is modest and below 100. The case of $d = 8$ mm [Figs. 5(c) and 5(d)] shows a good qualitative and quantitative agreement between numerical simulations and experimental measurements. In this case maximum separation correlates with the total electric dipole minimum at frequency 1.3 GHz [see white dashed line in Figs. 5(c) and 5(d)], where the separation coefficient achieves values of 600. This result experimentally proves the proposed concept of the effective magnetoelectric separation relying on anapole-type states.

VI. CONCLUSION

The concept of the magnetoelectric field separation in high-index dielectric tubes was proposed and analyzed. The core of the effect relies on the destructive interference between the displacement currents corresponding to different multipolar contributions. In particular, electric dipole and electric toroidal dipole moments cancel each other, giving rise to the anapole-type states. Careful design of these states with the help of the system's parameter variation enables superior suppression of the electric field in the center of the structure while the amplitude of the magnetic field is maximized at the same point. As it is shown in the paper, maximal separation corresponds, namely, to the anapole-type states, but not to the magnetic resonances of the structure. In the paper, the parameters under optimization for the tubes were the height of the tubes, the inner and outer radii, and the distance between the tubes. Uneven separations could be useful for an additional optimization of the separation factor, just like other geometrical and material parameters of the system, which were not involved in the optimization procedure. However, our point was to propose as simple a structure as possible with a rather high value of the separation coefficient, therefore we considered a solid tube and a system of some (no more than three) equal tubes only. Here the distance between the tubes was considered as one parameter among possible optimization characteristics providing an additional degree of freedom for the system, and being a proof that the separation could be further enhanced. Actually, it appeared to be a quite effective way to increase the separation (it becomes about 1.5 times stronger) in comparison with a standalone cylinder. The optimal distance was found to be 26 nm for silicon tubes in the visible range, which corresponds to the maximal obtained separation coefficient of ~ 6000, and 8 mm for given ceramic tubes. The theory is supported by a model microwave-range experiment, where silicon is replaced by ceramics. For the experimental structure, the anapole-based magnetoelectric separation is predicted to be near 600 (owing to the fabrication limitations), which fits the measurements of the local electric and magnetic field amplitudes.

Tunable and efficient spatial separation of the electric and magnetic fields of visible and infrared light has applications in a range of spectroscopic tests (e.g., in the sensing of magnetic transitions of atoms), and has numerous applications in metrology, sensing, fluorescent imaging, and many other areas.

ACKNOWLEDGMENTS

The calculations of multipole moments have been supported by the Russian Science Foundation (Grant No. 17-72-10230), The Government of the Russian Federation (Grant No. 08-08), and Deutsche Forschungsgemeinschaft (Project No. EV 220/2-1). A.S. acknowledges the support of Ministry of Education and Science of the Russian Federation (GOSZADANIE Grant No. 3.4982.2017/6.7). Special thanks to Egor Gurvitz for the multipolar decomposition schematics drawing. P.G. acknowledges support from PAZY foundation (Grant No. 01021248). This research was supported by a grant from the United States–Israel Binational Science Foundation and the NSF.

APPENDIX

It is well known that multipole decomposition could be represented in electric field or displacement currents formalisms, which are fully equivalent [1]. The relation between them can be expressed in the form of the following simple formula:

$$\mathbf{j} = \frac{\partial(\varepsilon_0 \varepsilon_p \mathbf{E})}{\partial t}, \tag{A1}$$

where $\mathbf{j}$ is the displacement current density, $\mathbf{E}$ is the electric field, ε_0 is the vacuum permittivity, and ε_p is the relative permittivity of a particle.

In our paper we speak about displacement currents to better understand the formation of the resulting field distribution (Fig. 1). However, the multipole decomposition and scattering cross-section calculations are done in the electric field formalism, following Ref. [41], because the numerical calculations in this case appear to be a little bit simpler. Expressions for the leading terms in irreducible Cartesian multipoles representation (up to the electric octupole moment) appear below:

Electric dipole moment:

$$\mathbf{p} = \varepsilon_0(\varepsilon_p - \varepsilon_d) \int \mathbf{E}(\mathbf{r}')d\mathbf{r}'. \tag{A2}$$

Electric quadrupole moment:

$$\hat{Q} = 3\varepsilon_0(\varepsilon_p - \varepsilon_d) \times \int \left[\mathbf{r}'\mathbf{E}(\mathbf{r}') + \mathbf{E}(\mathbf{r}')\mathbf{r}' - \frac{2}{3}[\mathbf{r}' \cdot \mathbf{E}(\mathbf{r}')]\hat{U}\right]d\mathbf{r}'. \tag{A3}$$

Magnetic dipole moment:

$$\mathbf{m} = 3\varepsilon_0(\varepsilon_p - \varepsilon_d) \int [\mathbf{r}' \times \mathbf{E}(\mathbf{r}')]d\mathbf{r}'. \tag{A4}$$

Magnetic quadrupole moment:

$$\hat{M} = \frac{\omega}{3i}\varepsilon_0(\varepsilon_p - \varepsilon_d) \int \{[\mathbf{r}' \times \mathbf{E}(\mathbf{r}')]\mathbf{r}' + \mathbf{r}'[\mathbf{r}' \times \mathbf{E}(\mathbf{r}')]\}d\mathbf{r}'. \tag{A5}$$

Electric octupole moment:

$$O_{\beta\gamma\tau} = \varepsilon_0(\varepsilon_p - \varepsilon_d) \times \left(\left\{\int [\mathbf{E}(\mathbf{r}')\mathbf{r}'\mathbf{r}' + \mathbf{r}'\mathbf{E}(\mathbf{r}')\mathbf{r}' + \mathbf{r}'\mathbf{r}'\mathbf{E}(\mathbf{r}')]d\mathbf{r}'\right\}_{\beta\gamma\tau} - (\delta_{\beta\gamma}\Lambda_\tau + \delta_{\beta\tau}\Lambda_\gamma + \delta_{\gamma\tau}\Lambda_\beta)\right). \tag{A6}$$

Electric toroidal dipole moment:

$$\mathbf{T} = \frac{i\omega}{10}\varepsilon_0(\varepsilon_p - \varepsilon_d) \int \{2\mathbf{r}'^2\mathbf{E}(\mathbf{r}') - [\mathbf{r}' \cdot \mathbf{E}(\mathbf{r}')]\mathbf{r}'\}d\mathbf{r}'. \tag{A7}$$

All integrations are performed over a particle's volume; $\mathbf{r}'$ denotes the radius vector, $\mathbf{E}(\mathbf{r}')$ denotes the electric field in the particle's volume, $\delta_{\alpha\beta}$ is the Kronecker delta, $\hat{U}$ is the unity matrix, and the auxiliary function $\mathbf{\Lambda}$ used in Eq. (6) is

$$\mathbf{\Lambda} = \frac{1}{5}\int \{2[\mathbf{r}' \cdot \mathbf{E}(\mathbf{r}')]\mathbf{r}' + (\mathbf{r}')^2\mathbf{E}(\mathbf{r}')\}d\mathbf{r}'.$$

It is worth noting that this representation implies the explicit separation between electric dipole and electric toroidal dipole moments that can be summed up as the total electric dipolar response:

$$\mathbf{D} = \mathbf{p} + \frac{ik_0}{c}\varepsilon_d\mathbf{T}, \tag{A8}$$

where k_0 is the wave vector in vacuum, c is the speed of light in vacuum, and ε_d is the dielectric constant of a surrounding environment ($\varepsilon_d = 1$ in the considered case).

The multipole contributions to a scattering cross-section appear below:

$$\text{Total electric dipole contribution}: \frac{k_0^4\sqrt{\varepsilon_d}}{12\pi\varepsilon_0^2 c\mu_0}|\mathbf{D}|^2. \tag{A9}$$

$$\text{Electric quadrupole contribution}: \frac{k_0^6\varepsilon_d\sqrt{\varepsilon_d}}{1440\pi\varepsilon_0^2 c\mu_0}\sum|Q_{\alpha\beta}|^2. \tag{A10}$$

$$\text{Magnetic dipole contribution}: \frac{k_0^4\varepsilon_d\sqrt{\varepsilon_d}}{12\pi\varepsilon_0 c}|\mathbf{m}|^2. \tag{A11}$$

$$\text{Magnetic quadrupole contribution}: \frac{k_0^6\varepsilon_d^2\sqrt{\varepsilon_d}}{160\pi\varepsilon_0 c}\sum|M_{\alpha\beta}|^2. \tag{A12}$$

$$\text{Electric octupole contribution}: \frac{k_0^8\varepsilon_d^2\sqrt{\varepsilon_d}}{3780\pi\varepsilon_0^2 c\mu_0}\sum|O_{\alpha\beta\gamma}|^2. \tag{A13}$$

Expressions (A2)–(A13) are employed for carrying out all the calculations reported in the paper.

[1] J. D. Jackson, *Classical Electrodynamics* (Wiley, New York, 1998).

[2] M. O. Scully and M. S. Zubairy, *Quantum Optics* (Cambridge University, Cambridge, England, 1997).

[3] C. J. Foot, *Atomic Physics* (Oxford University, Oxford, 2005).

[4] O. Deutschbein, Experimentelle untersuchungen über die Vorgänge bei der licht-emission, Ann. Phys. **428**, 183 (1939).

[5] M. Kasperczyk, S. Person, D. Ananias, L. D. Carlos, and L. Novotny, Excitation of Magnetic Dipole Transitions at Optical Frequencies, Phys. Rev. Lett. **114**, 163903 (2015).

[6] S. Karaveli and R. Zia, Spectral Tuning by Selective Enhancement of Electric and Magnetic Dipole Emission, Phys. Rev. Lett. **106**, 193004 (2011).

[7] T. Feng, Y. Xu, Z. Liang, and W. Hang, Optically-induced magnetic resonance in all-dielectric hollow nanodisk for tailoring magnetic and electric dipole emission, Opt. Lett. **41**, 5011 (2016).

[8] R. Regmi, J. Berthelot, P. M. Winkler, M. Mivelle, J. Proust, F. Bedu, I. Ozerov, T. Begou, J. Lumeau, H. Rigneault, M. F. García-Parajó, S. Bidault, J. Wenger, and N. Bonod, All-dielectric silicon nanogap antennas to enhance the fluorescence of single molecules, Nano Lett. **16**, 5143 (2016).

[9] M. K. Schmidt, R. Esteban, J. J. Sáenz, I. Suárez-Lacalle, S. Mackowski, and J. Aizpurua, Dielectric antennas: A suitable platform for controlling magnetic dipolar emission, Opt. Express **20**, 13636 (2012).

[10] B. Rolly, B. Bebey, S. Bidault, B. Stout, and N. Bonod, Promoting magnetic dipolar transition in trivalent lanthanide ions with lossless mie resonances, Phys. Rev. B **85**, 245432 (2012).

[11] D. G. Baranov, R. S. Savelev, S. V. Li, A. E. Krasnok, and A. Alù, Modifying magnetic dipole spontaneous emission with nanophotonic structures, Laser Photonics Rev. **11**, 1600268 (2017).

[12] A. Alù and N. Engheta, Achieving transparency with plasmonic and metamaterial coatings, Phys. Rev. E **72**, 016623 (2005).

[13] D. S. Filonov, A. S. Shalin, I. Iorsh, P. A. Belov, and P. Ginzburg, Controlling electromagnetic scattering with wire metamaterial resonators, J. Opt. Soc. Am. A **33**1910 (2016).

[14] A. S. Shalin, P. Ginzburg, A. A. Orlov, I. Iorsh, P. A. Belov, Y. S. Kivshar, and A. V. Zayats, Scattering suppression from arbitrary objects in spatially dispersive layered metamaterials, Phys. Rev. B **91**, 125426 (2015).

[15] T. H. Taminiau, S. Karaveli, N. F. Van Hulst, and R. Zia, Quantifying the magnetic nature of light emission, Nat. Commun. **3**, 979 (2012).

[16] H. Giessen and R. Vogelgesang, Glimpsing the weak magnetic field of light, Science **326**, 529 (2009).

[17] M. Burresi, D. Van Oosten T. Kampfrath, H. Schoenmaker, R. Heideman, A. Leinse, and L. Kuipers, Probing the magnetic field of light at optical frequencies, Science **326**, 550 (2009).

[18] A. Andreychenko, H. Kroeze, D. W. Klomp, J. J. Lagendijk, P. R. Luijten, and C. A. van den Berg, Coaxial waveguide for travelling wave MRI at ultrahigh fields, Magn. Reson. Med. **70**, 875 (2013).

[19] A. A. Mikhailovskaya, A. V. Shchelokova, D. A. Dobrykh, I. V. Sushkov, A. P. Slobozhanyuk, and A. Webb, A new quadrature annular resonator for 3 T MRI based on artificial-dielectrics, J. Magn. Reson. **291**, 47 (2018).

[20] H. E. Ives and T. C. Fry, Standing light waves: Repetition of an experiment by wiener, using a photoelectric probe surface, J. Opt. Soc. Am. **23**, 73 (1933).

[21] Y. Tang and A. E. Cohen, Enhanced enantioselectivity in excitation of chiral molecules by superchiral light, Science **332**, 333 (2011).

[22] E. Le Coarer, S. Blaize, P. Benech, I. Stefanon, A. Morand, G. Lérondel, G. Leblond, P. Kern, J. M. Fedeli, and P. Royer, Wavelength-scale stationary-wave integrated fourier-transform spectrometry, Nat. Photonics **1**, 473 (2007).

[23] M. Bashkansky, D. Park, and F. K. Fatemi, Azimuthally and radially polarized light with a nematic SLM, Opt. Express **18**, 212 (2010).

[24] G. Scott, Efficient generation of nearly diffraction-free beams using an axicon, Opt. Eng. **31**, 2640 (1992).

[25] S. Gomez-Graña, A. Le Beulze, M. Treguer-Delapierre, S. Mornet, E. Duguet, E. Grana, E. Cloutet, G. Hadziioannou, J. Leng, J. B. Salmon, V. G. Kravets, A. N. Grigorenko, N. A. Peyyety, V. Ponsinet, P. Richetti, A. Baron, D. Torrente, and P. Barois, Hierarchical self-assembly of a bulk metamaterial enables isotropic magnetic permeability at optical frequencies, Mater. Horiz. **3**, 596 (2016).

[26] S. N. Sheikholeslami, H. Alaeian, A. L. Koh, and J. A. Dionne, A metafluid exhibiting strong optical magnetism, Nano Lett. **13**4137 (2013).

[27] D. Markovich, K. Baryshnikova, A. Shalin, A. Samusev, A. Krasnok, P. Belov, and P. Ginzburg, Enhancement of artificial magnetism via resonant bianisotropy, Sci. Rep. **6**, 22546 (2016).

[28] A. B. Evlyukhin, S. M. Novikov, U. Zywietz, R. L. Eriksen, C. Reinhardt, S. I. Bozhevolnyi, and B. N. Chichkov, Demonstration of magnetic dipole resonances of dielectric nanospheres in the visible region, Nano Lett. **12**, 3749 (2012).

[29] D. L. Markovich, P. Ginzburg, A. K. Samusev, P. A. Belov, and A. V. Zayats, Magnetic dipole radiation tailored by substrates: Numerical investigation, Opt. Express **22**, 10693 (2014).

[30] S. Jahani and Z. Jacob, All-dielectric metamaterials, Nat. Nanotechnol. **11**, 23 (2016).

[31] A. I. Kuznetsov, A. E. Miroshnichenko, Y. H. Fu, J. Zhang, and B. Luk'yanchuk, Magnetic light, Sci. Rep. **2**, 492 (2012).

[32] A. B. Evlyukhin, C. Reinhardt, and B. N. Chichkov, Multipole light scattering by nonspherical nanoparticles in the discrete dipole approximation, Phys. Rev. B **84**, 235429 (2011).

[33] D. J. Traviss, M. K. Schmidt, J. Aizpurua, and O. L. Muskens, Antenna resonances in low aspect ratio semiconductor nanowires, Opt. Express **23**, 22771 (2015).

[34] C. Wu, N. Arju, G. Kelp, J. Fan, J. Dominguez, E. Gonzales, E. Tutuc, I. Brener, and G. Shvets, Spectrally selective chiral silicon metasurfaces based on infrared Fano resonances, Nat. Commun. **5**, 3892 (2014).

[35] K. E. Chong, B. Hopkins, I. Staude, A. E. Miroshnichenko, J. Dominguez, M. Decker, D. N. Neshev, I. Brener, and Y. S. Kivshar, Observation of Fano resonances in all-dielectric nanoparticle oligomers, Small **10**, 1985 (2014).

[36] I. Liberal, I. Ederra, R. Gonzalo, and R. W. Ziolkowski, Optical trapping in the presence of higher order mode sources and interactions, J. Opt. **16**, 114024 (2014).

[37] P. D. Terekhov, K. V. Baryshnikova, A. S. Shalin, A. Karabchevsky, and A. B. Evlyukhin, Resonant forward scattering of light by high-refractive-index dielectric nanoparticles with toroidal dipole contribution, Opt. Lett. **42**, 835 (2017).

[38] M. Caldarola, P. Albella, E.Cortés, M. Rahmani, T. Roschuk, G. Grinblat, R. F. Oulton, A. V. Bragas, and S. A. Maier, Non-plasmonic nanoantennas for surface enhanced spectroscopies with ultra-low heat conversion, Nat. Commun. **6**, 7915 (2015).

[39] A. E. Krasnok, C. R. Simovski, P. A. Belov, and Y. S. Kivshar, Superdirective dielectric nanoantennas, Nanoscale, **6**, 7354 (2014).

[40] A. E. Miroshnichenko, A. B. Evlyukhin, Y. F. Yu, R. M. Bakker, A. Chipouline, A. I. Kuznetsov, B. Luk'yanchuk, B. N. Chichkov, and Y. S. Kivshar, Nonradiating anapole modes in dielectric nanoparticles, Nat. Commun. **6**, 9069 (2015).

[41] A. Mirzaei, A. E. Miroshnichenko, I. V. Shadrivov, and Y. S. Kivshar, All-dielectric multilayer cylindrical structures for invisibility cloaking, Sci. Rep. **5**, 9574 (2015).

[42] G. Boudarham, R. Abdeddaim, and N. Bonod, Enhancing the magnetic field intensity with a dielectric gap antenna, Appl. Phys. Lett. **104**, 021117 (2014).

[43] W. C. Zhai, T. Z. Qiao, D. J. Cai, W. J.Wang, J. D. Chen, Z. H. Chen, and S. D. Liu, Anticrossing double Fano resonances generated in metallic/dielectric hybrid nanostructures using nonradiative anapole modes for enhanced nonlinear optical effects, Opt. Express **24**, 27858 (2016).

[44] A. B. Evlyukhin, T. Fischer, C. Reinhardt, and B. N. Chichkov, Optical theorem and multipole scattering of light by arbitrary shaped nanoparticles, Phys. Rev. B **94**, 205434 (2016).

[45] D. S. Filonov, A. E. Krasnok, A. P. Slobozhanyuk, P. V. Kapitanova, E. A. Nenasheva, Y. S. Kivshar, and P. A. Belov, Experimental verification of the concept of all-dielectric nanoantennas, Appl. Phys. Lett. **100**, 201113 (2012).

[46] P. D. Terekhov, K. V. Baryshnikova, Y. A. Artemyev, A. Karabchevsky, A. S. Shalin, and A. B. Evlyukhin, Multipolar response of nonspherical silicon nanoparticles in the visible and near-infrared spectral ranges, Phys. Rev. B **96**, 035443 (2017).